International Nano Letters (2019) 9:339–348
https://doi.org/10.1007/s40089-019-00289-3

ORIGINAL ARTICLE

The surface effect on the thermodynamic stability, half-metallic and optical properties of $Co_2MnGa(001)$ films: a DFT study

R. Ashtari Faregh[1] · A. Boochani[2] · S. R. Masharian[1] · F. H. Jafarpour[3]

Received: 21 July 2019 / Accepted: 31 October 2019 / Published online: 7 November 2019

Abstract

In this study, the half-metallic properties, thermodynamic stability and optical parameters of the full-Heusler Co_2MnGa compound and its four different terminations of Co–Co, Co–Mn, Mn–Ga and Co–Ga from the surface of Co_2MnGa (001) have been calculated based on the density functional theory (DFT). The results confirm the ferromagnetic half-metallic behavior with a magnetic moment of 4.08 μ_B and a gap of 0.32 eV at the Fermi level of Co_2MnGa bulk phase having a Cu_2MnAl-type structure. The density of states curves showed that all possible terminations from the Co_2MnGa (001) surface eliminate the half-metallic behavior except the termination of Mn–Ga case. Moreover, the results indicate that the termination of Mn–Ga with the lowest surface energy is the most stable termination for the application in spintronics. The optical coefficients such as real and imaginary dielectric function, refraction, extinction, energy loss function, optical conductivity and reflections of the bulk and Mn–Ga termination have been calculated and compared.

Keywords DFT · Co_2MnGa film surface · Thermodynamic phase diagram · Half-metal · Optical properties

Introduction

Many of novel aspects of the Heusler alloys in industries such as spintronics, microelectronics and electromechanics [1–3] have revealed the necessity of producing these compounds in the films form. The growth of Heusler films is a serious challenge in research due to the emergence of the structural disorders. Local disorders are major barriers to achieving 100% spin polarization in nanostructures made of layers of Heusler compounds. Hence, the theoretical and experimental study of the half-metallic behavior of the Heusler thin films has been the sketch of many researches [4–6]. Yet, controlling the structural disorders is still an important issue to achieve applicable films with unique properties, just like samples with perfect order.

The half-Heusler compound NiMnSb with half-metallic behavior was discovered in about 1983 [7]. However, cobalt-based full-Heusler compounds showing full spin polarization have only been known for a few years. Full-Heusler alloys with X_2YZ chemical formula and various physical properties, depending on the composition, might be metal, semiconductor or semi-metal, but many of them are ferromagnetic. High-spin polarized Heusler ferromagnetisms seem to be ideal for applications in giant magneto-resistance (GMR) and tunneling magneto-resistance in magnetic tunneling junctions (MTJs). [8] Among these, Co_2MnAl films may be introduced as ideal candidates for high-sensitive Hall sensors due to the unusual inherent Hall conductance [9–11]. So far, reports have been presented on the study of layered structure samples of Co_2YZ (Y = Mn, Cr, Fe, Z = Al, Si, Ga). For example, the effects of structural order on the transport and magnetic properties of Co_2MnGa have been investigated, as well as the process of growth of these films with amorphous structures, and also their structural order improvement. [12–15]. In this group of Heusler compounds, Manganese is the main element, because one can say that the most known ferromagnetic Heuslers, except CrO_2, are Mn-based compounds. Recent studies on Co_2MnX (X = Si, Ge, Sn) and their films by Raphael et al. [5, 6, 16–18] predicted that the thin films of these compounds are not half-metallic

✉ A. Boochani
arash_bch@yahoo.com

[1] Department of Physics, Hamedan Branch, Islamic Azad University, Hamedan, Iran

[2] Department of Physics, Kermanshah Branch, Islamic Azad University, Kermanshah, Iran

[3] Physics Department, Bu-Ali Sina University, Hamedan 65174-4161, Iran

ferromagnetic, or that their full spin polarization is limited by antisite defects [19–25]. Hence, in this work, the half-metallic behavior of Co_2MnGa thin films is discussed, and the results of the study of the electrical and optical properties and thermodynamic stability of the 4 different terminations from Co_2MnGa (001) surface are presented as well as a comparison with its bulk state. In Sect. 2, we express the calculation methods in details. Sections 3.1–3.3 discuss the properties of the bulk state of the Heusler compound Co_2MnGa, its (001) surface, and the optical properties of the bulk and surface cases, respectively; and finally, Sect. 4 is the conclusions.

Calculation methods and models

The calculations were performed based on the density functional theory (DFT) implemented in Wien2K computational package, using the electronic full potential linear augmented plane waves method (FP-LAPW) [26, 27], and the generalized gradient approximation (GGA) was applied to obtain the exchange–correlation interaction potential [28]. The energy and forces on each atom were converged with 1×10^4 eV/atom and 0.02 eV/Å. Also, the optimized cutoff energy, RK_{max}, lmax and KPoint were selected as − 6, 8 Ry, 10 and 3000, respectively.

Results

The bulk Heusler Co_2MnGa properties

After optimizing the lattice parameters through energy minimization, the full-Heusler compound Co_2MnGa was crystallized in a cubic structure $L2_1$ with the Cu_2MnAl-type Fm-3m space group and the equilibrium lattice constant of 5.695 Å. We also found that Co_2MnGa is a ferromagnetic compound with a total magnetic momentum 4.08 μ_B according to Slider–Pauling's relation $\mu_t = Z_t - 18$ [29, 30]. These values are in agreement with the results of others' calculations [4, 31].

The primitive $L2_1$ structure consists of four FCC sublattices merged together with the atomic positions as: Co-I (0.25, 0.25, 0.25), Co-II (0.75, 0.75, 0.75), Ta (0.5, 0.5, 0.5) and, Z (0,0,0) depicted in Fig. 1. Also, the Hg_2CuTi-type structure is another schema in this phase, which consists of four non-equivalent atomic positions with a fourfold symmetry in the space group F4-3m including Co-I (0, 0, 0), Co-II (0.25, 0.25, 0.25), Ta (0.5.0.5.0.5), and Z (0.75, 0.75, 0.75).

To understand the electronic structure of the bulk Co_2MnGa, the total and partial density of states (DOS) as well as the energy band structure are presented in Fig. 2. From the total DOS curve, it is found that Co_2MnGa can

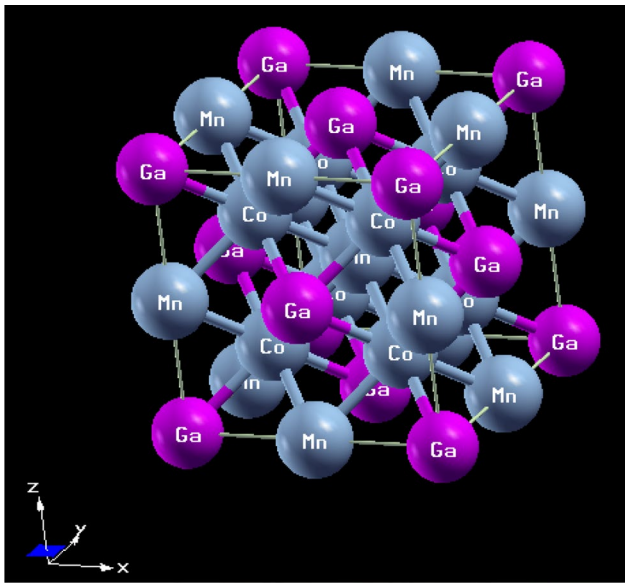

Fig. 1 The Cu_2MnAl-type crystal structure of Co_2MnGa

almost be considered as a ferromagnetic half-metal with the spin polarization close to 100% at the Fermi level. According to the band structure curve in both the majority and minority spins, the band-width below the Fermi level from about − 4 to 0 eV is due to the strong hybridization of the Mn-3d and Co-3*d* electrons in the occupied valence levels. The band structure of the majority spin strongly shows metallic behavior; while in the minority spin, the maximum valence level is almost above the Fermi level which results in a gap of 0.32 eV and approximately semiconducting behavior of this compound.

According to the partial DOS curves, the highest electron contribution at the Fermi level which corresponds to the Slater–Pauling rule belongs to Mn and Co, and these two atoms are the origin of half-metallic behavior at the Fermi level. However, the electron contribution of Ga atoms is connected to the semi-core region, i.e., the range of (− 10 to 7 eV). Also, the localization of the states in the DOS diagram at the conduction region shows that the electronic contribution of the orbital d to the Mn and Co atoms in this range is very high, and the interaction between the *d*–*d* bonds of these two atoms and the *p*–*d* bonds of Ga and Mn atoms leads to this spin splitting at the Fermi level.

Properties of the (001) surfaces

The Co_2MnGa Heusler structure was cut along the Miller planes (001), and 20 angstroms vacuum were applied in parallel to direction of the crystal growth symmetrically at the two ends of the film. Then, four ideal structures were obtained with Co–Co, Co–Mn, Mn–Ga and Co–Ga terminations containing 9 atomic layers. The lattice constants of

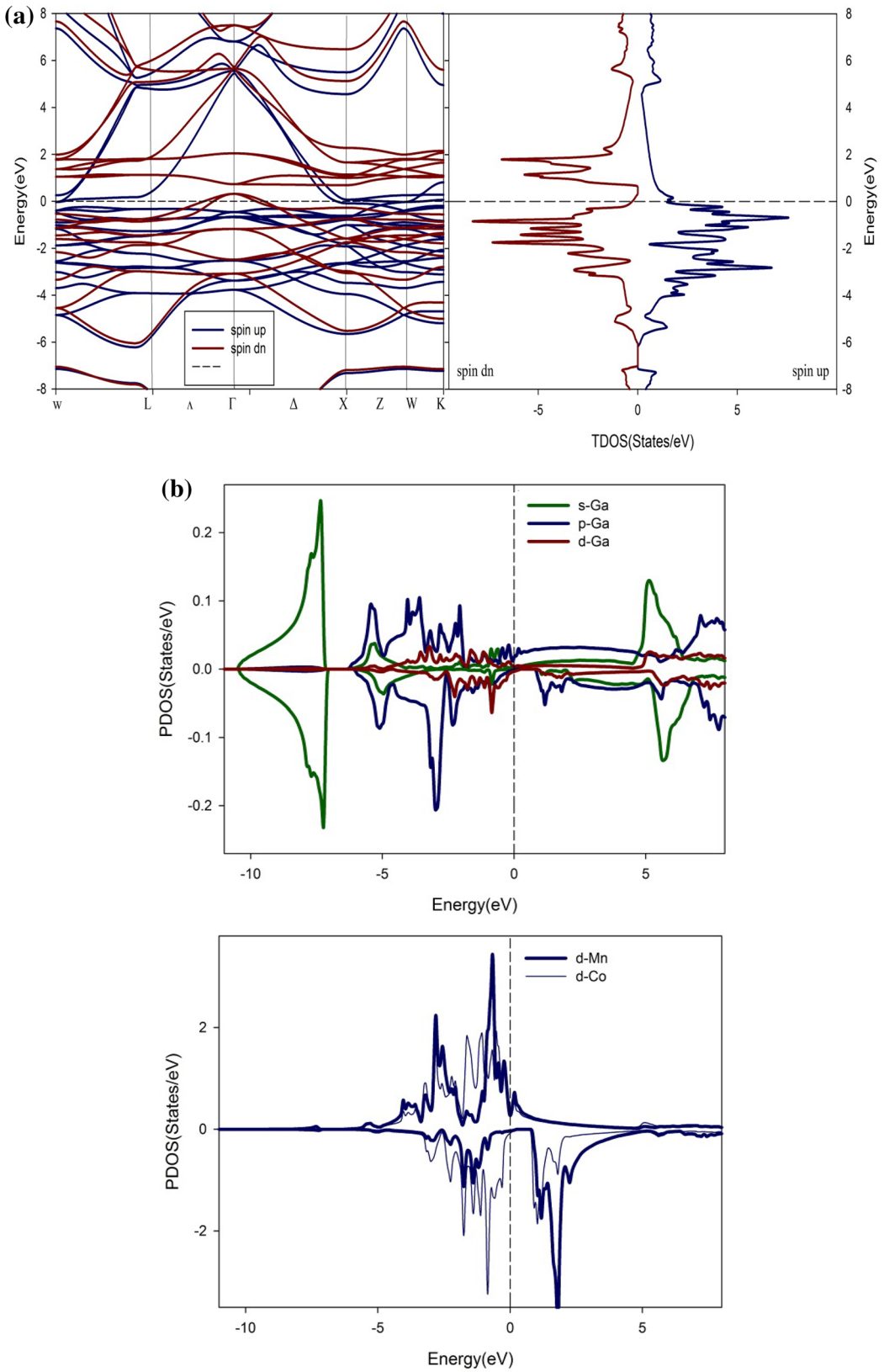

Fig. 2 **a** The total density of states and band structure curves of the bulk Co_2MnGa. **b** The partial density of states of Ga atom, and the contribution to the d orbital of Mn and Co atoms in the bulk Co_2MnGa

these films are $\left(\frac{a}{2}\sqrt{2}\right)$, where $a = 5.695$ Å is the equilibrium lattice constant of the bulk Co_2MnGa. Figure 3 depicts the side view of these terminations. We relaxed the atomic layers by minimizing the total energy and atomic forces.

Surfaces' stability

As we know, surfaces' stability is an important factor in the growth of thin films. A lower surface energy means that the surface will be more stable [32]. To study the relative stability of the different terminations, we calculated the surface's free energy as a function of atomic chemical potentials in the framework of the atomic thermodynamics theory. The surface's free energy is calculated as follows:

$$\gamma = \frac{1}{2A}\left[G - \sum_i \left(N_i \mu_i\right)\right], \tag{1}$$

where G and A are the film's total energy and total surface's area, respectively. N_i and μ_i are the number chemical potential of the ith atom in the sliced layers. The sum of these chemical potentials is equal to the Gibbs free energy of the bulk Co_2MnGa, since it is assumed that the films' surfaces are in the thermodynamic equilibrium with the middle layers, i.e.,

$$2\mu_{Co} + \mu E + \mu_{Ga} = G_{Co_2MnGa} \tag{2}$$

By removing μ_{Ga} from Eq. 2, we can obtain the surface's free energy relation in terms of μ_{Mn} and μ_{Co}. The maximum chemical potentials of the Mn and Co atoms are obtained from their bulk structures, and their minimum chemical potentials are determined in such a way that by decreasing μ_{Mn} and μ_{Co}, Co and Mn leave the structure and Co_2Ga and MnGa structures are produced.

$$\frac{1}{2}\left(G_{Co_2MnGa} - G_{MnGa}\right) \le \mu_{Co} \le G_{Co} \tag{3}$$

$$G_{Co_2MnGa} - G_{Co_2Ga} \le \mu_{Mn} \le G_{Mn} \tag{4}$$

The results of phase diagram show that all of the four terminations are achievable. Since the phase transition point of

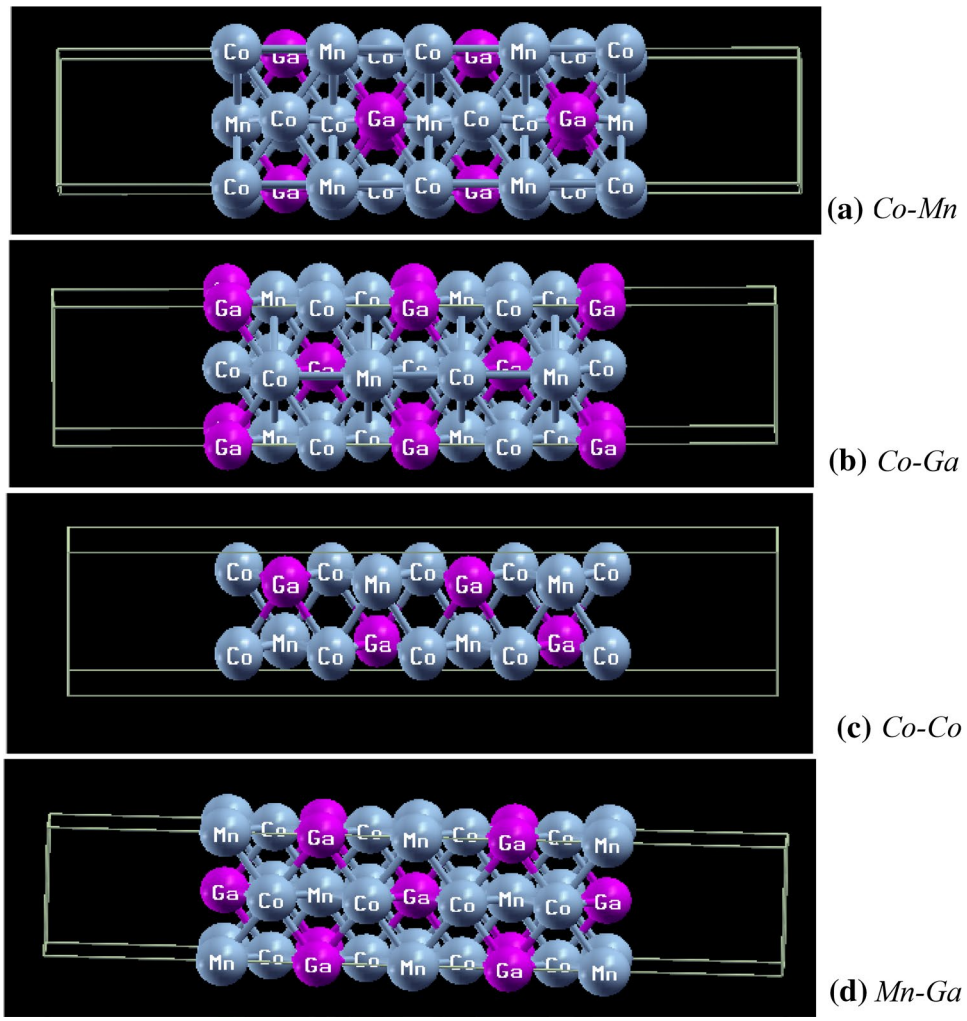

Fig. 3 **a–d** Four different terminations of the (001) surface of Co_2MnGa

these terminations is within the allowed range of the phase diagram, it is concluded that the Co_2MnGa bulk structure is also thermodynamically stable. Among the terminations of Co_2MnGa (001) surface, the Mn–Ga termination with the lowest surface free energy is the most stable one, and the Co–Co termination is the most unstable surface with the highest free energy (see Fig. 4).

The electronic properties of surfaces

The total density of states curves of Co_2MnGa (001) surfaces with Co–Co, Co–Mn, Mn–Ga and Co–Ga terminations are shown in Fig. 5a. As can be seen, among the four terminations, only the Mn–Ga termination conserves an approximately half-metallic behavior with a spin polarization of about 94 percent. However, other three terminations of Co–Co, Co–Mn and Co–Ga have spin polarization rates of about 83, 51, and 75%, respectively. Because the distance of the intermediate layers in these films are similar to the bulk system, the atomic density of states of these middle layers matches the corresponding atoms in the bulk structure, and it is observed that at each of the four terminations, the electronic localization below the Fermi level corresponds to the orbits *d* of Co, Mn and orbital *p* of Ga atom.

From the band structure that is shown in Fig. 5b, for the termination Mn–Ga, the strong metallic behavior in spin up, and the partial presence of energy levels above the Fermi level and the reception of a small indirect gap of 0.2 eV in spin down confirm the nearly half-metallic behavior in the bulk state. To more precisely study the surface electronic behavior, the atomic DOS curves of the surface and intermediate layers of this termination are shown in Fig. 6. The electronic states contribution to the Mn atom in the surface layer far exceed the one in the intermediate layer at the Fermi level, and basically, the surface effects on the Mn atoms in the surface layer have led to this magnetic anisotropy, so that splitting of the states is observed in the minority spin. However, it is further observed that the contribution of Ga to magnetic anisotropy at the Fermi level is very small, and the main density of the states of these atoms belongs to the core region (the energy range from − 7 to − 10 eV). An even more interesting point is that in the valence band in the range of (− 3 to − 5 eV) of the middle and sub-surface Co atoms, the electronic states' behavior are almost homogeneous and completely non-magnetic. However, in the Fermi region, we see an increase in the electronic states, which is due to the localization of Co electronic states at the film's surface.

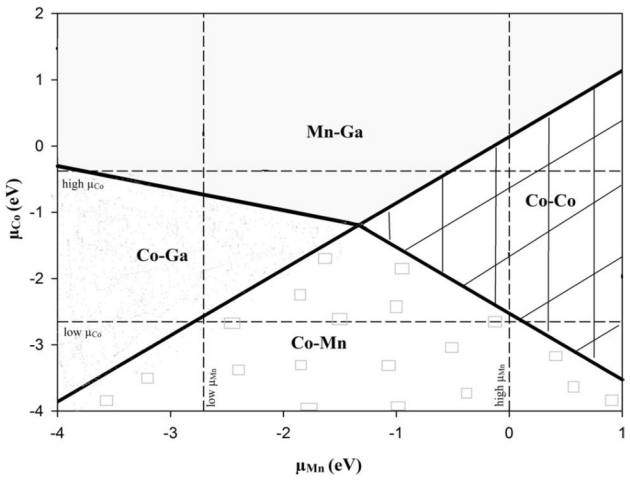

Fig. 4 The phase diagram of the surface terminations Co_2MnGa (001)

Optical properties of the bulk and surfaces

In the following, we study the optical parameters for Co_2MnGa bulk and the Mn–Ga termination of Co2MnGa (001) surface in Figs. 7a–g. Since in the bulk mode, due to symmetry, the crystal is completely homogeneous in different states, so we only plot the *x*-axis direction.

In the curve of the real part of dielectric function ($\varepsilon(\omega)$) in Fig. 7a, the similarity of the optical behavior between the bulk state and the Mn–Ga termination is quite clear. The static dielectric function of the bulk Co_2MnGa tends to negative infinity, which is a proof of the metallic behavior of this compound in this interval of energy, while in the Mn–Ga termination along *x*, it reached a constant value of − 18. Along *x*-axis, the general form of $Re\varepsilon(\omega)$ of Mn–Ga termination is similar to the bulk state, except that the response rate of this mono-layer to the incident light is far greater than its bulk state, and it is even more in the areas where the sign of $\varepsilon_x(\omega)$ is positive. In the *z* direction, the response of Mn–Ga termination to the incident light is quite positive and different from the *x*-axis. In the region of 0–12 eV, the response of the matter to the light decreases with increasing energy of the incident photon, and there is no distinction between *x* and *z* directions in $Re\varepsilon(\omega)$ after 12 eV.

Figure 7b shows the $Im\varepsilon(\omega)$ curve for the bulk and Mn–Ga termination of Co_2MnGa. In the bulk state, the static values of this function tend to infinity, which is a solid proof of its metallic behavior and that it has intra-band optical transitions. As seen in the figure, due to the metallic nature of this compound, most of the transitions occur in the infrared and visible regions, and by increasing the energy of the incident photon at the edge of UV, the intensity of transitions decreases, and practically after 12 eV, no transition is observed for this material and it passes light entirely. But in Mn–Ga termination, $Im\varepsilon(\omega)$ is completely anisotropic in two directions *x* and *z* at low energies, so that in the *x* direction, its behavior is similar to the bulk state with lesser intensities of transitions in the energies of 1.3, 2.2 eV; while in the *z* direction, some peaks are emerged with increasing the

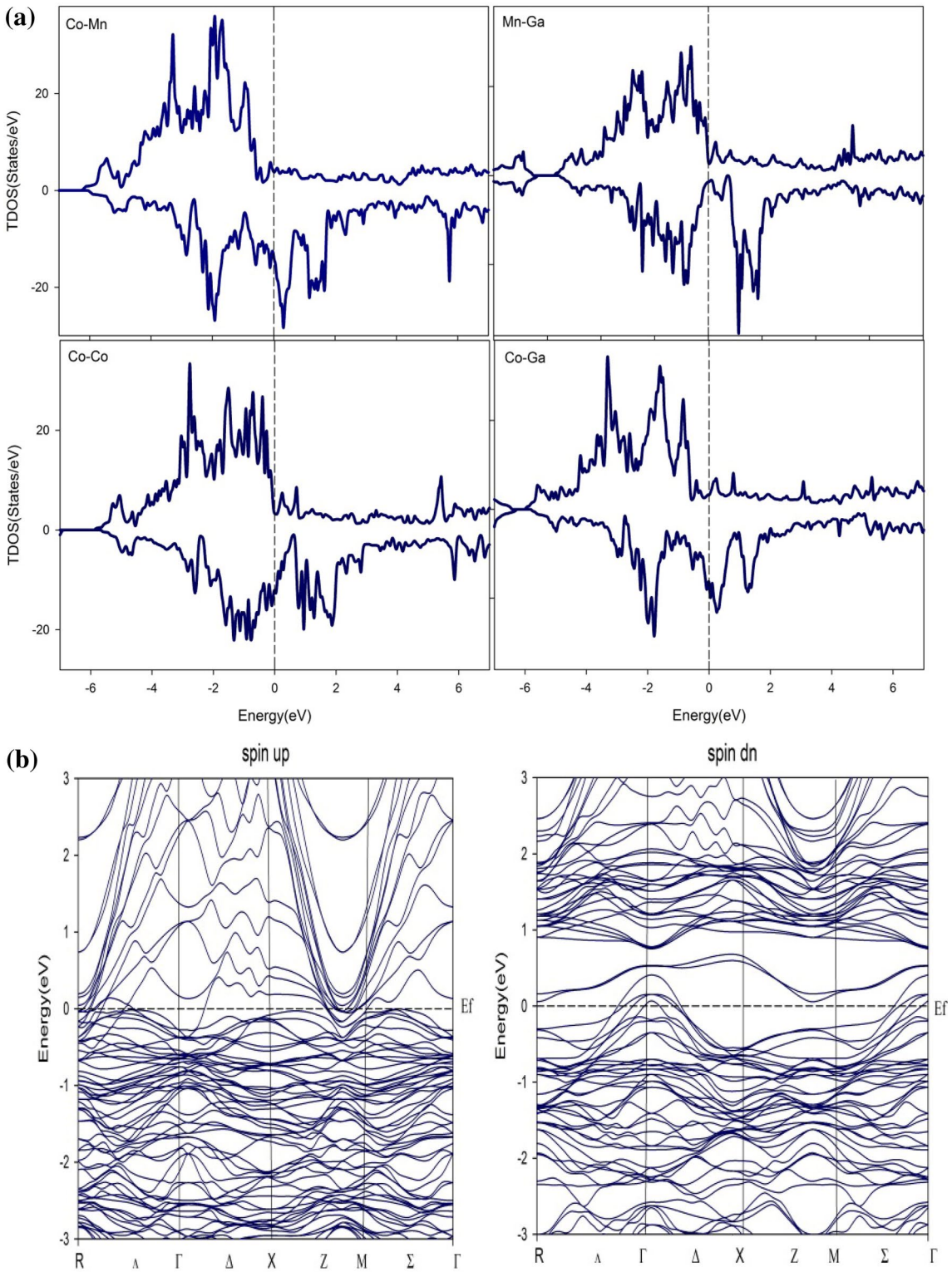

Fig. 5 **a** The total density of states curve of the terminations Mn–Ga, Co–Mn, Co–Co, and Co–Ga. **b** The energy band structure of the Mn–Ga termination

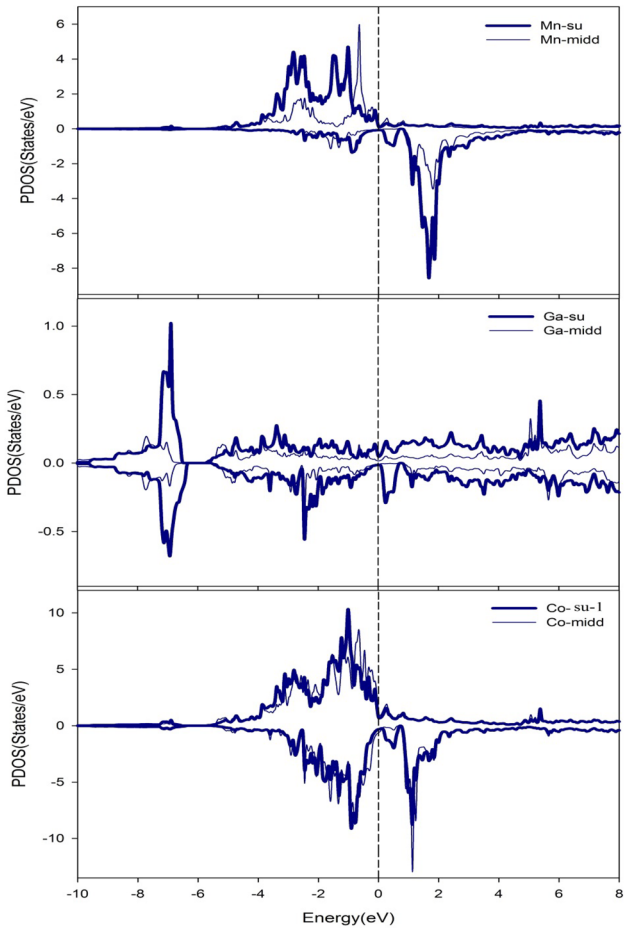

Fig. 6 The partial density of states curve of Co, Mn, and Ga atoms in the Mn–Ga termination

energy of incident photon at 0.9 eV, 1.5 eV, and 2.5 eV. In both directions, $Im\varepsilon(\omega)$ tends to zero at high energies. In Fig. 7c, we see the energy loss function ($L(\omega)$) curve, which represents the amount of energy loss of the incident photon. For the bulk Co_2MnGa, all optical regions practically do not show a significant drop in the incident energy other than the energy of about 22 eV, which has a very sharp Dirac peak. In the curve of the loss function for the Mn–Ga termination, it is observed that the Dirac peak of the bulk state is destroyed and in both directions the curve has a broadening. In both x and z directions, more than one peak is observed with lower intensities than the bulk Co_2MnGa, and these peaks represent the roots of the $Re\varepsilon(\omega)$ in the x and z directions.

We consider the refractive index in Fig. 7d. For the bulk Co_2MnGa, according to our expectation of metallic behavior of this compound, the static refractive index tends to large quantities, because in these energies and in the infrared region, electrons of this metal can easily be excited by incident light. By increasing the energy of the incident photon and entering the visible region, the refractive index decreases. Moreover, in the refractive index curve of the Mn–Ga termination, we see that in low energies, the refractive index is anisotropic in the two directions of x, z. It is worth considering the above issues of the metallic behavior of the Mn–Ga termination along x, which is also clear here, so that, in low energies, the high refractive index confirms this metallic behavior, but with increasing intensity of the incident photon, the refraction of light decreases in both x and z directions. In the z direction, the static refractive index is about 6, which suggests the semiconductivity behavior of the compound in this direction. After 10 eV energy, the refraction indexes are lower than one that indicated the super luminance phenomena.

The reflection index curve is observed in Fig. 7e, the general form of which for Mn–Ga termination with less intensity is similar to the bulk state. The static value of the reflection index for the bulk Co_2MnGa and the Mn–Ga termination along x direction is about 95%, i.e., a very strong metal in this direction. After about 10 eV, the reflection coefficient is shifted toward long peaks; so in these energies, most of the incident light is reflected.

The extinction coefficient is a measure of light absorption in matter. In Fig. 7f, the extinction coefficient curves of bulk Co_2MnGa and its Mn–Ga termination similarly show that the maximum extinction coefficient occurs in the infrared region and at zero energy limit, which is due to the metallic nature of the matter. However, with the increase in the energy of the incident photon, the amount of extinction coefficient intensely decreases to the range of 1 eV, then continue decreasing but with a lower rate. As shown in the reflection coefficient curve, the reflectance in this region is about 50%. At the energy level of 3.2 eV, An characteristic peak for both the bulk and Mn–Ga termination is observed along x, which is equivalent to the root of $Re\varepsilon(\omega)$ in this energy. Moreover, in the z direction, for the Mn–Ga termination, we see three peaks in the visible area and the UV edge (at 0.8 eV, 2.1 eV and 3.1 eV, respectively). After 9 eV, the curves of the extinction coefficient are symmetric in both directions, overlap and tend to zero. In Fig. 7g, it is observed that the optical conductivity coefficient has a very high value, due to the occurrence of metallic behavior in the bulk and the Mn–Ga termination along x at zero energy, which is in agreement with the graph of $Re\varepsilon(\omega)$. In the energy range of (1.5–10 eV), simultaneously with the absorption of incident light, we observe the optical transitions increase in both the bulk and Mn–Ga termination, which results in the highest absorption and optical conductivity in the visible and ultraviolet spectral range. Based on the zero amount of the energy loss function in the lower energies and high $Im\varepsilon(\omega)$, it is shown that these compositions are good sensitive to the light with high absorption. Also, the zero amount of the $Im\varepsilon(\omega)$ and extinction coefficients are referred to the transparent behavior for these compounds.

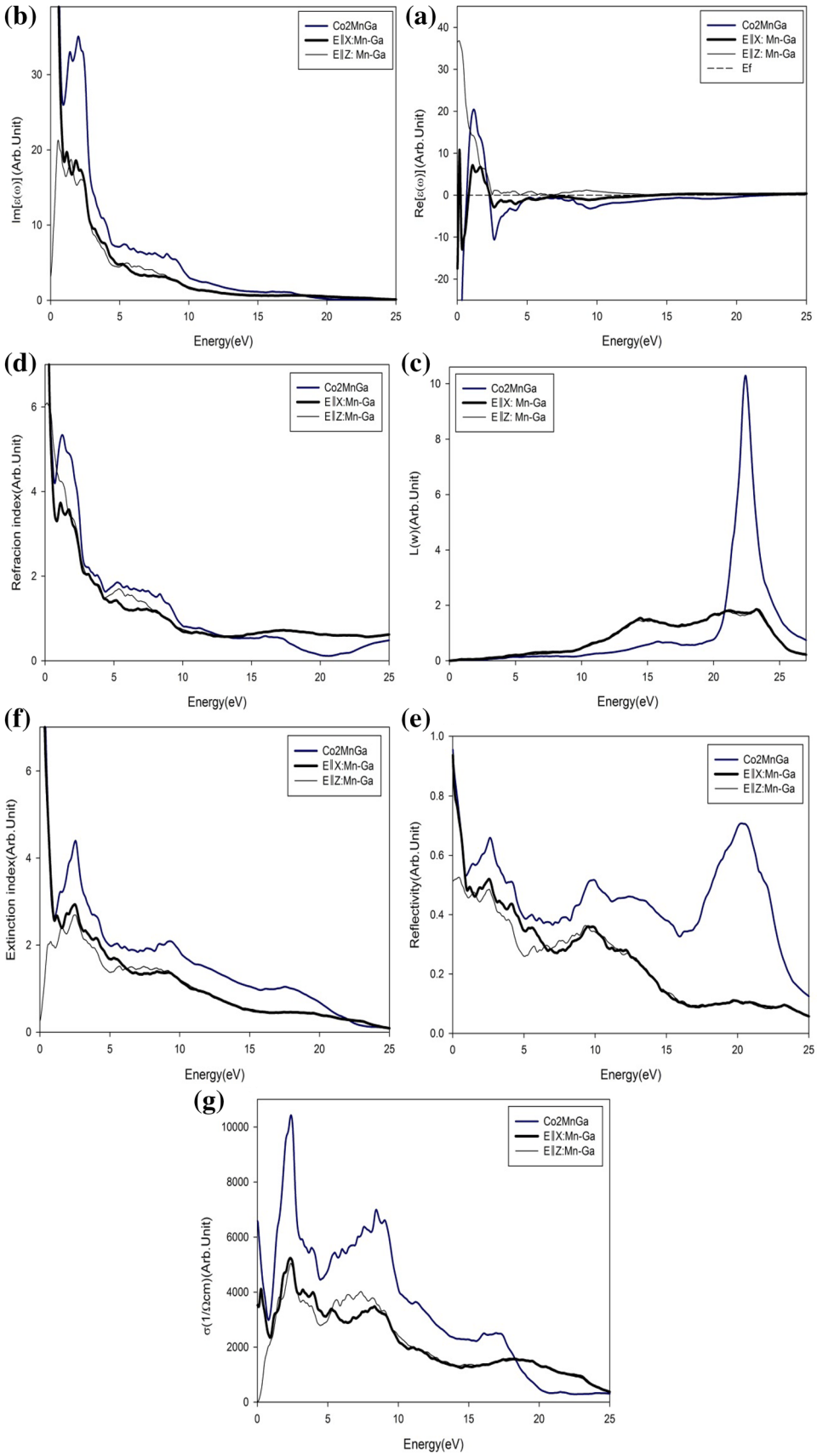

Fig. 7 **a**, **b** The real and imaginary parts of dielectric function, **c** the electron energy loss function, **d** refraction index, **e**, **f** reflection and extinction index, **g** the optical conductivity coefficient of the bulk Co_2MnGa and Mn–Ga termination

Conclusion

The thermodynamic stability, the structural, electronic and optical properties of the four terminations of Co–Co, Co–Mn, Mn–Ga, and Co–Ga from Co_2MnGa (001) surface were studied using the first principles calculations. Calculations are based on DFT framework and GGA approximation. The spin polarized calculations showed that the bulk Co_2MnGa is nearly a half-metal with a spin polarization of less than 100 with a magnetic moment of 4.08 μ_B; among the all terminations, only the Mn–Ga termination retains this property. The Mn–Ga termination is the most stable thin film due to the lowest surface free energy and the most suitable for maintaining the spin injection property in spintronic devices. Examination of the bulk Co_2MnGa and its Mn–Ga termination reflects the similarity of optical behavior in these two structures.

References

1. Mao, G.Y., Liu, X.X., Gao, Q., Li, L., Xie, H.H., Lei, G., Deng, J.B.: Effect of As and Nb doping on the magnetic properties for quaternary Heusler alloy FeCoZrGe. J. Magn. Magn. Mater. **398**, 1–6 (2016)
2. Xie, H.H., Gao, Q., Li, L., Lei, G., Mao, G.Y., Hu, X.R., Deng, J.B.: First-principles study of four quaternary Heusler alloys *ZrMnVZ* and *ZrCoFeZ* (*Z* = *Si, Ge*). Comput. Mater. Sci. **103**, 52–55 (2015)
3. Vasil'ev, A.N., Buchel'nikov, V.D., Takagi, T., Khovailo, V.V., Estrin, E.I.: Shape memory ferromagnets. Phys. Usp. **46**, 559 (2003)
4. Dubowik, J., Gościańska, I., Szlaferek, A., Kudryavtsev, Y.V.: Films of Heusler alloys. Mater. Sci. Pol. **25**, 583–598 (2007)
5. Singh, L.J., Barber, Z.H.: Structural, magnetic, and transport properties of thin films of the Heusler alloy Co2*MnSi*. Appl. Phys. Lett. **84**, 2367 (2004)
6. Picozzi, S., Continenza, A.: Co2MnX.(X = Si, Ge, Sn). Heusler compounds: an ab initio study of their structural, electronic, and magnetic properties at zero and elevated pressure. Phys. Rev. B **66**, 094421 (2002)
7. De Groot, R.A., Mueller, F.M., Van Engen, P.G., Buschow, K.H.J.: New Class of materials: half-metallic ferromagnets. Phys. Rev. Lett. **50**, 2024 (1983)
8. Oogane, M., et al.: Large tunnel magnetoresistance in magnetic tunnel junctions Co2 MnX (X = Al, Si) Heusler alloys. J. Phys. D Appl. Phys. **39**, 834–841 (2006)
9. Kubler, J., Felser, C.: Berry curvature and the anomalous Hall effect in Heusler compounds. Phys. Rev. B **85**, 012405 (2012)
10. Tung, J.C., Guo, G.Y.: High spin polarization of the anomalous Hall current in *Co*-based Heusler compounds. New J. Phys. **15**, 033014 (2013)
11. Zhu, L.J., Zhao, J.H.: Anomalous resistivity upturn in epitaxial L21-Co2 MnAl films. Sci. Rep. **7**, 42931 (2017)
12. Fujii, S., Ishida, S., Asano, S.: Electronic and magnetic properties of $X_2Mn_{1-x}V_xSi$ (X = Fe and Co). J. Phys. Soc. Jpn. **63**, 1881–1888 (1994)
13. Hütten, A., Kammerer, S., Schmalhorst, J., Reiss, G.: Half-metallic alloys. In: Galanakis, I., Dederichs, P.H. (eds.) Fundamentals and Applications, pp. 241–264. Springer-Verlag, Berlin (2005)
14. Sakuraba, Y., Miyakoshi, T., Oogane, M., Ando, Y., Sakuma, A., Miyazaki, T.: Direct observation of half-metallic energy gap in Co2 *MnSi* by tunneling conductance spectroscopy. Appl. Phys. Lett. **89**, 052508 (2006)
15. Kudryavtsev, Y.V., Oksenenko, V.A., Kulagin, V.A., Dubowik, J., Lee, Y.P.: Ferromagnetic resonance in Co_2MnGa films with various structural ordering. J. Magn. Magn. Mater. **310**(2), 2271–2273 (2007)
16. Fecher, G.H., Kandpal, H.C., Wurmehl, S., Morais, J., Lin, H.J.: Design of magnetic materials: the electronic structure of the ordered, doped Heusler compound $Co_2Cr_{1-x}Fe_xAl$. J. Phys. Condens. Matter. **17**, 7237 (2005)
17. Kübler, J., William, A.R., Sommers, C.B.: Formation and coupling of magnetic moments in Heusler alloys. Phys. Rev. B **28**, 1745 (1983)
18. Ökoğlu, G.G., Gülseren, O.G.: Electronic structure of half-metallic ferromagnet Co2*MnSi* at high-pressure. Eur Phys J **J76**, 321–326 (2010)
19. Boochani, A., Khosravi, H., Khodadadi, J., Solaymani, S., Majidiyan, M., Sarmazdeh, Taghavi, R., Sayed, M., Elahi, M.: Calculation of half-metal, debye and curie temperatures of Co_2VAl compound: first principles study. Commun. Theoret. Phys. **63**(5), 641 (2015)
20. Majidi, S., Achour, A., Rai, D.P., Nayebi, P., Solaymani, S., Nezafat, N.B., Elahi, S.M.: Effect of point defects on the electronic density states of SnC nanosheets: first-principles calculations. Results Phys. **7**, 3209–3215 (2017)
21. Achour, H., Achour, A., Solaymani, S., Islam, M., Vizireanu, S., Arman, A., Ahmadpourian, A., Dinescu, G.: Plasma surface functionalization of boron nitride nano-sheets. Diam. Relat. Mater. **77**, 110–115 (2017)
22. Solaymani, S., Kulesza, S., Ţălu, Ş., Bramowicz, M., Nezafat, N.B., Dalouji, V., Rezaee, S., Karami, H., Malekzadeh, M., Dorbidi, E.S.: The effect of different laser irradiation on rugometric and microtopographic features in zirconia ceramics: study of surface statistical metrics. J. Alloy. Compd. **765**, 180–185 (2018)
23. Ţălu, Ş., Bramowicz, M., Kulesza, S., Dalouji, V., Solaymani, S., Valedbagi, S.: Fractal features of carbon–nickel composite thin films. Microsc. Res. Tech. **79**(12), 1208–1213 (2016)
24. Ţălu, Ş., Bramowicz, M., Kulesza, S., Ghaderi, A., Dalouji, V., Solaymani, S., Khalaj, Z.: Microstructure and micromorphology of Cu/Co nanoparticles: surface texture analysis. Electron. Mater. Lett. **12**(5), 580–588 (2016)
25. Ţălu, S., Bramowicz, S., Kulesza, S., Shafiekhani, A., Ghaderi, A., Mashayekhi, F., Solaymani, S.: Microstructure and tribological properties of FeNPs@a-C: H films by micromorphology analysis and fractal geometry. J Ind Eng Chem **43**, 164–169 (2016)
26. Blaha, P., Schwarz, K., Madsen, G.K.H., Hvasnicka, D., Luitz, J.: WIEN2 k, An augmented plane wave local orbitals program for calculating crystal properties. Austria: Karlheinz Schwarz, Techn. Universit Wien, ISBN 3-9501031-1-2. (2001)
27. Kresse, G., Furthmüller, J.: Efficiency of ab initio total energy calculations for metals and semiconductors using a plane-wave basis set. Comput. Mater. Sci. **6**, 15–50 (1996)
28. Perdew, J.P., Burke, K., Ernzerhof, M.: Generalized gradient approximation made simple. Phys. Rev. Lett. **77**, 3865 (1996)

29. Skaftouros, S., Özdoğan, K., Şaşıoğlu, E., Galanakis, I.: Generalized Slater-Pauling rule for the inverse Heusler compounds. Phys. Rev. B **87**, 024420 (2013)
30. Jung, D., Koo, H.J., Whangbo, M.H.: Study of the 18-electron band gap and ferromagnetismin semi-Heusler compounds by non-spin-polarized electronic band structure calculations. THEOCHEM **527**, 113–119 (2000)
31. Sargolzaei, M., Richter, M., Koepernik, K., Opahle, I., Eschrig, H.: Spin and orbital magnetism in full Heusler alloys: a density functional theory study of Co2YZ (Y = Mn, Fe; Z = Al, Si, Ga, Ge). Phys. Rev. B **74**, 224410 (2006)
32. Han, H.P., Gao, G.Y., Yao, K.L.: Preserving stable 100% spin polarization at (111) heterostructures of half-metallic Heusler alloy Co_2VGa with semiconductor PbS. J. Appl. Phys. **112**, 083710 (2012)